Structure and domain formation in ferroelectric thin films

Vlooswijk, Ard H.G.

Chapter 4

Lead titanate thin films under "small" compressive strain: $PbTiO_3$ on $SrTiO_3(001)_c$

Parts of this chapter are published as:
S. Venkatesan, A. Vlooswijk, B.J. Kooi, A. Morelli, G. Palasantzas, J.T.M. de Hosson and B. Noheda – "Monodomain strained ferroelectric $PbTiO_3$ thin films: Phase transition and critical thickness study", *Physical Review B*, vol. **78**, no. 10, 104112, September 2008.

4.1 Introduction

Because many applications of ferroelectrics require vertically accessible polarization, single c-oriented ferroelectric thin films are widely studied [39, 104, 105, 106]. In section 2.5 and 3.5 we have shown that $PbTiO_3$ thin films on $SrTiO_3$ in principle belong to this category. As shown in Figure 2.4 and calculated by Pertsev et al. [33], thin films of $PbTiO_3$ on $SrTiO_3$ are expected to be under compressive strain and, indeed, c-oriented. There are several reasons to study $PbTiO_3/SrTiO_3$, of which the most important ones are the well-established chemical and thermal treatment of $SrTiO_3$ substrates and the experimental good lattice fit between $SrTiO_3$ and $PbTiO_3$ at room temperature. Despite the large efforts, the behavior of these thin films is still not fully understood. The domain formation in $PbTiO_3$ often plays an important role in the interpretation of the ferroelectric behavior. Therefore, the thickness of the thin film is a crucial parameter to define the ferroelectric response. After all, as long as the film is thin enough, the misfit is accommodated by lattice strain and not by other effects like domain formation (twinning), dislocation formation etc. The question of "what is thin enough?", or in other words "what is the critical thickness for strain relaxation?" is therefore very important. This critical thickness can be calculated using different thermodynamic models, like the Matthews-Blakeslee [2] and People-Bean [3] model. In the next section these two models and their applicability will be treated

in more detail. For the case of $PbTiO_3$ on $SrTiO_3$ (using literature bulk values [41, 107]), a small compressive misfit exists at the growth temperatures that we have employed. The order of magnitude of this misfit is such that it allows for a relatively large critical thickness for strain relaxation. In this chapter, we show that a critical thickness far beyond those predicted by the previously-mentioned models can be obtained in this film-substrate system and we explain the reasons. It should be reminded though, that the misfit strain shifts T_c upwards, giving rise to modifications in Figure 3.6. This shift of T_c also raises the question whether our films are grown in the paraelectric or ferroelectric phase. Temperature-dependent XRD measurements which will be presented in section 4.4.1, show that our films are grown in the ferroelectric phase. This is an important observation, since the domain structure in a ferroelectric is strongly dependent on its thermal history, especially when ferroelectric/paraelectric phase transitions are involved.

The defining conditions of our thin $PbTiO_3$ layers on $SrTiO_3$, apart from their growth in the ferroelectric phase, the are the relatively slow cooling rate ($-5°$C/min) and the absence of electrodes. Thermodynamics is valid when the film is grown slow enough or thin enough for defects to annihilate during growth or post-annealing. Growth rates up to 2 Å/s, corresponding to a 5Hz laser frequency in combination with our deposition parameters, lead to thin films which are c-oriented, as is expected from thermodynamics. In these films, the presence of periodic 180° domains has been confirmed by XRD [1, 53, 106] and possibly also by AFM [108].

This is in agreement with other reports. In thin films with thicknesses below the critical thickness for strain relaxation and without electrodes, periodic 180° domains can be present. In the present work, also double diffraction peaks are observed by XRD, indicating a high quality coherent film/substrate interface. These double diffraction peaks only appear when certain requirements are met, of which a good lattice match, proper film thickness and a high quality coherent substrate/film interface are the most important ones. As far as we know, double diffraction in ferroelectric thin films has not been acknowledged in the literature, and these peaks are often misinterpreted as impurity phases [105, 109]. The piezoelectric constant of these films is measured by p-AFM to be in the order of 30 pm/V.

4.2 Thin film growth

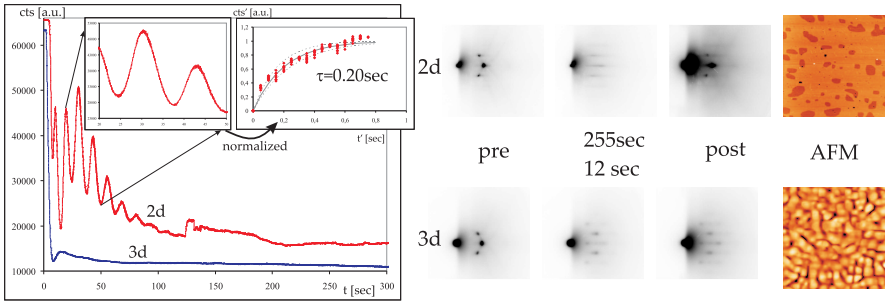

Figure 4.1: RHEED intensity as a function of growth time (left) and RHEED patterns of $PbTiO_3$ grown on (top center panels) a $0.02°$ miscut $SrTiO_3$ substrate with a 5Hz laser repetition rate showing oscillations and a 2d RHEED pattern characteristic for layer-by-layer and step-flow growth. And (bottom) on a $0.04°$ miscut substrate and a 10Hz laser repetition rate showing no oscillations and a RHEED pattern characteristic for 3d growth. The insets in the intensity versus time graph show a blow-up of the oscillations and a fit to the relaxation after every pulse. The dotted lines indicate the 95% uncertainty interval. Ex-situ $1 \times 1\mu m$ AFM images of the film surfaces are shown with z-scales of 3 nm (top) and 20 nm (bottom).

The growth of thin films of $PbTiO_3$ has been performed by pulsed laser ablation of in-house fabricated $PbTiO_3$ targets with a $2 - 7\%$ excess of lead. The deposition settings are listed in Table 3.1 in chapter 3 and in most cases we have used a spot size of $2.5mm^2$ and a target-substrate distance between 48 and 51mm. After deposition, samples were typically annealed in 500mbar of oxygen at their growth temperature and immediately cooled down with a -5°C/min cooling rate to room temperature. In order to achieve the earlier mentioned layer-by-layer growth, RHEED is used to monitor the adatom diffusion in time. As shown in the inset of Figure 4.1(left), for the growth of $PbTiO_3$ on single-terminated $SrTiO_3$ and on $SrRuO_3$ electroded $SrTiO_3$, the relaxation time constant τ, calculated with the use of formula 3.2 is of the order of 0.20 ± 0.04sec. This means that a laser repetition rate of 1Hz (and a spot size of $2.5mm^2$) allows enough time for adatom diffusion to ensure layer-by-layer growth, while laser repetition rates above 5Hz are expected not to do so.

When $PbTiO_3$ is grown with a 1Hz laser repetition rate, the RHEED os-

cillations still damp out with time. The rate at which they damp out is of the order of 10 monolayers, which is a common observation in heteroepitaxy of metal oxides by PLD [110]. Generally, the RHEED pattern remains that of a two-dimensional surface and does not turn into that of a rough three-dimensional surface, indicating that the growth mode changes to step-flow. This growth mode does not allow for in-situ real-time growth-rate and thickness monitoring, but it ensures a high film quality. Also shown in Figure 4.1 is what happens for growth rates above 5Hz and substrates with two terminations: the growth mode is three-dimensional and RHEED oscillations cannot be observed.

The substrate treatment, termination and miscut can be important parameters for the growth mode [111]. We have not studied these effects systematically. Instead, we have used mainly TiO_2-terminated $SrTiO_3$ substrates with 0.1-0.2° miscuts. The growth rate then seemed to be an important parameter in determining the formation of a-domains in thin films of $PbTiO_3$. Therefore, we have systematically varied the deposition rate by varying the laser frequency. Ex-situ AFM generally showed two types of surfaces of these thin films: Single c-domain oriented thin films showed atomically flat film surfaces with unit cell steps and some screw dislocations. These surfaces show that the films grow in a layer-by-layer or step-flow mode. Our RHEED observations indicate that after an initial layer-by-layer growth, the growth mode switched to step-flow (this is depicted in the top row of Figure 4.1, as described above). In some cases, we observed a so-called "mound" or "wedding cake" surface, indicating that after initial island growth, the growth mode switched to a layer-by-layer or step-flow mode.

A second type of morphology is found: In the cases of a-domain formation, we have observed thin films with rougher, but still relatively flat surfaces (RMS roughness below 5 nm).

These surfaces show a so-called "fingerprint" structure as depicted in the bottom row of Figure 4.1 (and even more clear in Figure 3.4 in chapter 3). In correspondence with these AFM observations, the RHEED intensity showed 3d features and no oscillations. For the thickest film without a-domains, we have detected a combination of these observations: a two dimensional RHEED pattern, but a fingerprint-like structure in AFM. This could indicate that the thickness of this film is very close to the critical thickness for formation of elastic 90° domains.

4.3 Thin film characterization

4.3.1 Double diffraction

As the surface-to-volume ratio of these thin films is very large, high quality interfaces are very important. While later in this chapter (Figure 4.10) we will show that the top surface of the thin films is of high quality, XRD measurements also show very good coherence between film and substrate and thus a high quality substrate/film interface. This is deduced from peaks as those observed at $q_\perp$=2.114 in Figure 4.2(a). This peak and similar peaks observed at $q_\perp = 1.062$ and $q_\perp = 1.933$ (Figure 4.3 [1]) are often misinterpreted as impurity phases or remain unexplained. This is certainly the case in Figure 8 by Dahl et al. [105] and Figure 1 in Gan et al. [109] and possibly also in Figure 1A by Stemmer et al. [112] and Figure 1 by S.B. Mi et al. [113]. But actually, these peaks are "double diffraction" or "Umweganregung" peaks, a very well-known phenomenon in electron diffraction, but relatively unknown in XRD. This is quite remarkable, since the use of X-ray diffraction to structurally characterize epitaxial thin films is well-established [94, 114]. Especially in a field like ferroelectrics, where (periodic) domains are of large importance, there is a lot of interest in looking at reciprocal space maps (and not only standard θ-2θ scans) in order to detect the presence of satellite peaks, possibly related to electrostatic domains [1, 53, 106], but also to crystallographic twinning domains [115] or impurity phases.

Information like the epitaxial relations and crystal quality are easily extracted using X-ray diffraction. The general model used is that of a simple superposition of two reciprocal lattices, but in reality this image is too simplistic. The epitaxial relationship between substrate and film, increases the possibility of simultaneous diffraction. And this simultaneous or "double diffraction", also known as "Umweganregung" should be taken into account, as it can give rise to satellite peaks. Especially in the kind of set-up we have used and which is quite commonly used in lab-diffractometry of thin films. We have used an X'Pert MRD in line focus; the slits in this set-up are narrow in the ω-direction (parallel to he scattering plane) but very broad in ϕ (perperdicular to the scattering plane). This results in a very limited res-

[1] Throughout this chapter, q-space is normalized to the room temperature $SrTiO_3$ lattice parameter (a=3.905 Å).

olution in that direction and any reflection perpendicular to the scattering plane, like Umweganregung peaks, can easily show up in the diffractograms. The "Umweganregung" peaks are generally weak and quite sharp. For our measurements performed at the synchrotron, this means the observation of "Umweganregung" peaks is less likely due to the better resolution, but when the proper diffraction conditions are met, the increased beam intensity allows to monitor even weak "Umweganregung" peaks. Simultaneous diffrac-

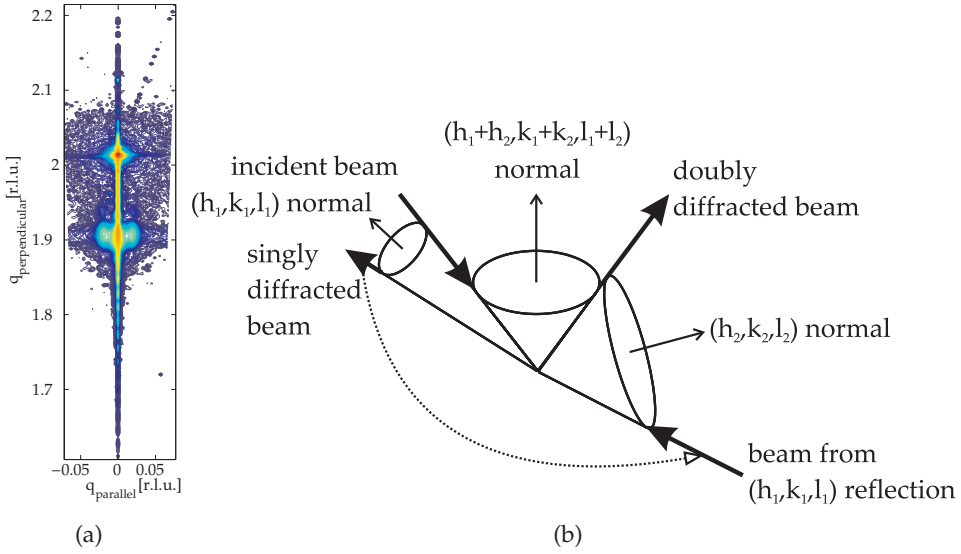

Figure 4.2: a) Q-space RSM[1] around the (002) Bragg peak of a 22 nm $PbTiO_3$ film on $SrTiO_3$. The peak at $q_\perp = 2.114(2)$ is constructed by double diffraction from the $SrTiO_3$ (004)- and $PbTiO_3$ (00$\bar{2}$)-plane. b) General idea of multiple diffraction in reciprocal space. The beam singly diffracted by the (h_1, k_1, l_1)-plane, acts as an incoming beam for the second diffraction by the (h_2, k_2, l_2)-plane. This results in a double diffraction peak, seemingly diffracted by the $(h_1 + h_2, k_1 + k_2, l_1 + l_2)$-plane.

tion occurs when two (or more) lattice points lie on the Ewald's sphere of reflection at the same time. For single crystals, thorough analysis can be found in literature [95, 116]. Although simultaneous diffraction in single crystals can change the strength of a Bragg peak, the peaks are always found at reciprocal lattice points. For a hybrid system like a heteroepitaxial thin film

on a substrate, a modified analysis is needed and can be found in recent literature [96]. The main difference with simultaneous diffraction from single crystals, is the fact that two distinct reciprocal lattices are superimposed. This can lead to sums of diffraction vectors which end up at positions that belong to neither of the two primary lattices. The general idea of multiple diffraction is presented in Figure 4.2(b). A typical combination of Bragg planes and their associated Bragg cones are shown with their apexes meeting at one point. Any beam obeying Bragg's law must lie along the surface of these cones. Multiple diffraction arises when an incident beam is obeying the Bragg condition for one set of planes and the resulting diffracted beam can act as an incoming beam for a second set of planes. The diffracted beam (h_1, k_1, l_1) has to lie on the cone of (h_2, k_2, l_2). With a limited ϕ resolution (rotation of the cone), the beam constructed by double diffraction is most easily observed, since it only has to have a length matching to the accompanying Ewald's sphere.

When double diffraction peaks are investigated using ray diagrams as in Figure 4.2(b), several aspects should be taken into account. First of all, any combination of a film and substrate reflection should obey the requirement that it will cross the film interface. This allows for two options: Either the beam is transmitted through the film, diffraction from the substrate occurs and this signal serves as an incoming beam for a film plane which diffracts outwards; or the beam is diffracted by the film and the diffracted beam acts as an incoming beam for a substrate plane which diffracts outwards. Second, beams (h_1, k_1, l_1) and (h_2, k_2, l_2) should be of comparable intensity. This means the thickness and quality of the film play a role. In epitaxial thin films, the signal coming from the substrate is in general very strong compared to the film. In double diffraction this means the signal from the film will be the limiting factor in the detection of a double diffraction peak and the film has to have a good crystallinity and a minimum thickness to give enough signal. On the other hand, in a thin film of $PbTiO_3$ with Pb being a very strong X-ray scatterer, the film should not be too thick, because this leads to very strong absorption of the incoming beam by the thin film. Additionally, if at the position of a double diffraction peak in reciprocal space, there are weak or no substrate or film peaks, the possibilities of observation of the double diffraction peak are best. And finally, concerning the construction of double diffraction peaks using the ray diagrams, the electron density of film and

substrate should be similar, otherwise a correction for the refractive index is needed.

Since $PbTiO_3$ and $SrTiO_3$ have similar electron densities, no correction for difference in refractive index is needed and ray diagrams can be used without any correction to predict the double diffraction peaks. Taking into account that the (101)-type reflections in perovskites are usually very strong, the "Umweganregungen" constructed from these reflections are the first ones to take into account. For the current case, the strength of the Bragg reflections at room temperature for $PbTiO_3$ and $SrTiO_3$ in order from strong to weak is summarized here:

material	strongest					weakest	
$PbTiO_3$ [41]	(101)	(110)	(111)	(100)	(211)	(200)	...
$SrTiO_3$ [107]	(110)	(200)	(211)	(111)	(220)	(310)	...

"Umweganregungen" constructed from these strong reflections are expected to be most easily observed. The peak positions in q-space (in relative lattice units, normalized with respect to the $SrTiO_3$ substrate lattice) are given by

$$\begin{array}{rcl} q_{\parallel} & = & \frac{a_{STO}}{a_{STO}}\sqrt{h_{STO}^2+k_{STO}^2}+\frac{a_{STO}}{a_{PTO}}\sqrt{h_{PTO}^2+k_{PTO}^2} \\ q_{\perp} & = & \frac{a_0}{c_{STO}}l_{STO}+\frac{a_{STO}}{c_{PTO}}l_{PTO} \end{array} \tag{4.1}$$

Where h, k and l are the Miller indexes, a, c_{STO} are the normalization lattice parameters and a_0 is the observed lattice parameter. If we index the Umweganregung as a sum of the indices of the two involved primary reflections, the (00L) Umweganregung peaks and their indices are expected to be[1] (in order of peak strength and based on bulk lattice parameters):

$PbTiO_3$	$SrTiO_3$	Umweganregung	$q_{\parallel}[r.l.u.]$	$q_{\perp}[r.l.u.]$
(101)	$(\bar{1}01)$	(002)	0	1.940
$(\bar{1}\bar{1}\bar{1})$	(112)	(001)	0	1.060
(111)	$(\bar{1}\bar{1}2)$	(003)	0	2.940
(101)	$(\bar{1}03)$	(004)	0	3.940
(002)	(002)	(004)	0	3.879

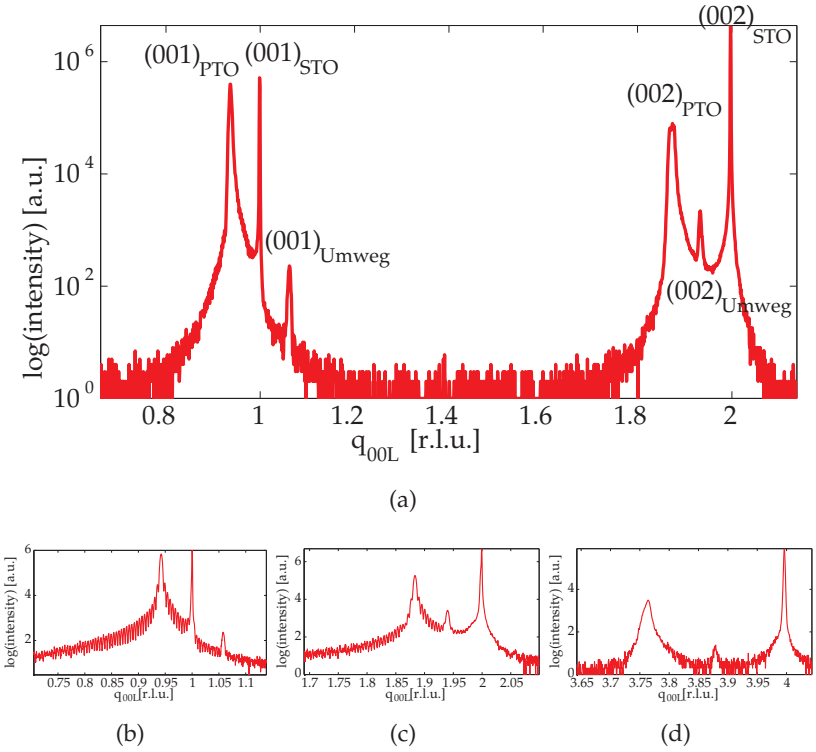

Figure 4.3: a) Linear scans along the [00L]-direction of a $PbTiO_3$ thin film on $SrTiO_3$ of 150 nm (a) and 82 nm (b-d). We have observed Umweganregung peaks for films with thicknesses ranging from 22 nm up to 150 nm. a) The indicated peak positions ((001) and (002)) correspond to $q_\perp = 1.000(2); 2.000(2)$ for $SrTiO_3$, $q_\perp = 0.936(2); 1.874(2)$ for $PbTiO_3$ and $q_\perp = 1.062(2); 1.933(2)$ for the Umweganregung peaks. b-d) The peak positions correspond to b) $q_\perp = 1.000(2); 0.942(2); 1.058(2)$; c) $q_\perp = 2.000(2); 1.883(2); 1.940(2)$ and d) $q_\perp = 4.000(2); 3.765(2); 3.880(2)$ for $SrTiO_3$, $PbTiO_3$ and Umweganregung, respectively.

Which is in good agreement with the measurements in Figure 4.3. Note that the zero-values for the Umweganregung a-lattice parameter, is valid due to the substrate/film coherence. Although this is not our case, when the film/substrate interface is incoherent, the peak due to double diffraction will end up outside the crystal truncation rod and gives quantitative information about the strain state [96].

By performing ϕ-rotation, we have confirmed that the observed peaks

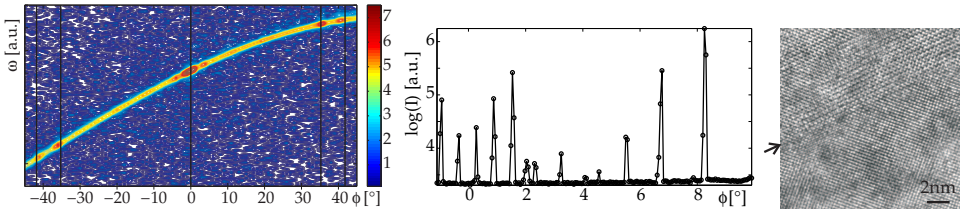

Figure 4.4: Signs of a high quality substrate/film interface by XRD and HRTEM. a) ω versus ϕ plot of the (002) double diffraction peak ($q_\perp = 1.940$ r.l.u.) in our laboratory diffractometer. The vertical lines indicate $\phi = 0°$(constructed from (00L)'s); $\phi = 35.3°$ (constructed from (11L)'s) and $\phi = 41.8°$ (constructed from (12L)'s) b) The same ϕ dependence recorded at beamline W1, Hasylab, showing a large amount of peaks. These peaks can be constructed by subsequent diffraction from the substrate and the thin film because of the good coherence between substrate and film. c) HRTEM of the interface between $SrTiO_3$ (bottom) and a 37 nm thin film of $PbTiO_3$ (top)[2]. This confirms the high quality of the interface (which is indicated by an arrow).

are due to double diffraction. Double diffraction peaks are strongly angle dependent and from single crystal Umweganregung it is known that rotation around the scattering vector shows very sharp peaks at certain positions. Therefore, while focussing on a (002) Umweganregung reflection, the sample has been rotated around ϕ (the azimuth) (and ω was rocked, which is necessary because the sample surface is not perfectly parallel to the x-ray beam in our lab diffractometer). The result is plotted in angle-space in Figure 4.4(a). For every omega rocking curve, the crystal truncation rod is crossed, leading to increased intensity (typically 10% of the intensity I_p of the main peak at $\phi = 0°$). At certain ϕ values the intensity is somewhat increased. Peaks are observed for $\phi = 0; \pm 4; \pm 36; \pm 40°$. The ϕ resolution ($1°$) does not allow us to draw definitive conclusions from these peak positions. The peak at $0°$ is the main peak and can be constructed from primary $(00L)$ reflections. Similarly, the peaks at $\pm 36°$ show an intensity of 0.25-0.30I_p and can be constructed from primary $(11L)$ reflections. The peak at $\pm 41°$, with 0.13-0.17I_p, can be constructed from primary $(12L)$ reflections, while the peak at $\pm 4°$ (0.17-0.18I_p) remains unexplained.

In principle, many peaks can be observed for different ϕ angles, but many of them are very weak. Synchrotron measurements as plotted in Figure 4.4(b) show that there are indeed many different peaks. We have not indexed these peaks, but we think that their presence indicates a very good substrate/film coherence with a sharp interface. This facilitates the construction of many double diffraction paths, even of relatively weak singly diffracted beams. The high quality of the interface is confirmed by HRTEM measurement as in Figure 4.4(c) [2].

4.3.2 Compositional properties

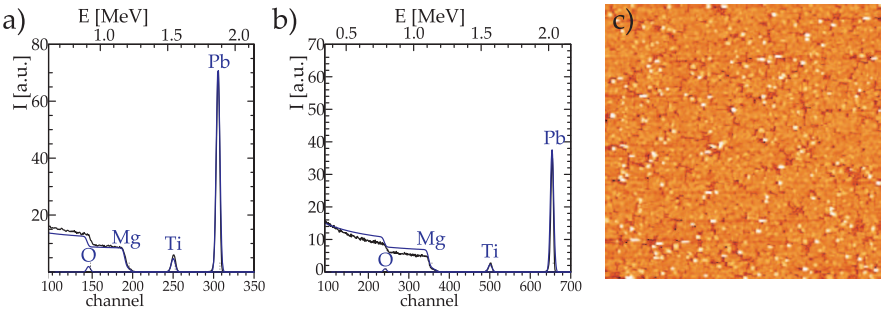

Figure 4.5: RBS measurement data and simulation of a 30 nm $PbTiO_3$ film grown on a MgO substrate with the detector at (a) $60°$ and (b) $10°$ from the incoming beam. The plotted simulations represent a 0.99:1.01 $Pb:Ti$-ratio. The two different beam directions deviate with a higher (a) and lower (b) $Pb:Ti$-ratio indicating that these deviations are most likely due to chanelling effects. c) is an AFM measurement of this film, showing a 3-dimensional structure of islands/platelets with a RMS roughness of $5nm$ (4×4 μm scan size; full z-scale 40 nm).

In order to verify the thin film composition, X-ray photoelectron spectroscopy (XPS) and Rutherford backscattering (RBS) have been used. Remarkably, XPS measurements consistently give a 2:1 Pb:Ti ratio, when composition standards are taken into account correctly. This observation is not fully understood, but the most likely explanation is that the topmost layer of the thin film is Pb-rich. Especially since this 2:1 ratio is not reproduced by RBS measurements. Although RBS measurements have been performed on

[2] TEM measurements performed by Sriram Venkatesan, Materials Science Group, University of Groningen, The Netherlands.

$PbTiO_3$ films on MgO (RBS does not allow for good quantitative measurements when heavy-element substrates are used), there are no straightforward reasons to expect large composition differences due to this difference in substrate. In order to prevent channeling effects [117], detectors at 10° and 60° with respect to the incoming beam have been used. Measurements on a 30 nm thick $PbTiO_3$ film on MgO with detectors at $10°$ and $60°$ is depicted in Figure 4.5(a-b). The measurements can be simulated using a 0.99:1.01 $Pb : Ti$-ratio showing opposite deviations for the two different beam directions. Therefore, it can be concluded that the $Pb : Ti$ ratio is 1:1 within measurement errors, which means that the excess lead in our PLD target is lost in the deposition process and the thin film is stoichiometric.

In combination with our XPS measurements and the fact that the probe depth of RBS is more than a factor of 10 larger than that of XPS, it is likely that the topmost monolayers of our thin films are Pb-rich. Both effects are consistent with existing literature: for thin films of $PbTiO_3$, a Pb-enriched surface layer is observed by XPS frequently [118]. And Kwak et al. [119], have shown RBS data on $PbTiO_3$ thin films on different substrates, showing stoichiometric compositions.

4.4 Results and discussion

4.4.1 90° domain formation: critical thickness and growth rate

Even though the experimental misfit strain at room temperature between $SrTiO_3$ and tetragonal $PbTiO_3$ is only of the order of 10^{-3}, misfit strain can certainly play an important role in this system due to the misfit with the cubic $PbTiO_3$. At our typical growth temperature of 570°C, the misfit strain is 0.01-0.02 (and compressive). On the one hand, this provides opportunities to study the effect of misfit strain by studying the temperature-dependent behavior. On the other hand, this misfit strain at elevated temperatures can give rise to dislocation, defect or domain formation.

Several reports are available of a/c-domains in $PbTiO_3$ on $SrTiO_3$ [94, 120], which show that when strain relaxation takes place in this system, a/c-domain formation is the most common mechanism. There are at least two possible reasons for this domain formation. The first one is intrinsic to the $PbTiO_3/SrTiO_3$ combination and related to the film thickness: If the film is

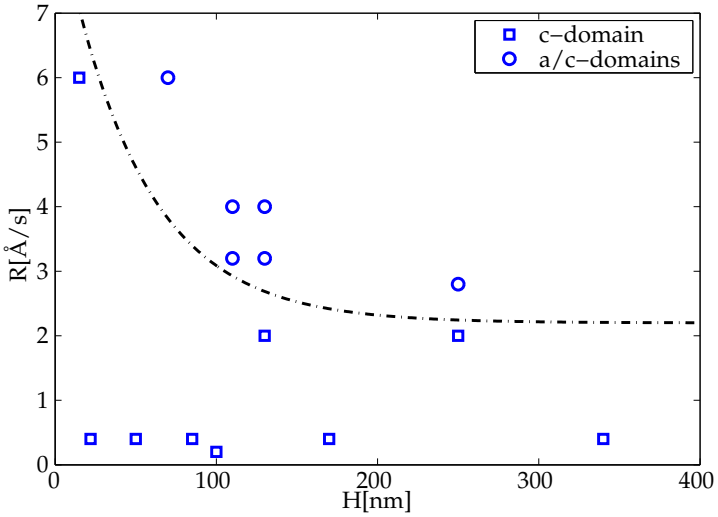

Figure 4.6: Growth rate R versus $PbTiO_3$ film thickness H showing the presence of single c-domain (squares) versus a/c-domains (circles) in the film. The domain structure has been observed by XRD and/or TEM. The growth rate R has been calculated by multiplying the laser repetition rate with an average growth rate per pulse of 0.4 Å. The dashed line is a guide to the eye to distinguish the regions with and without a-domains.

thicker than the critical thickness for strain relaxation, the strain will relax loosing coherence with the substrate, which makes a/c-domain formation plausible. The second reason is related to the growth rate of the thin film. When the film is grown very rapidly, chances of off-stoichiometry and other growth-imperfections increase. This induces randomness in the thin film, increasing the chances for nucleation of a-domains, resulting in a/c-domain formation.

Remarkably, the critical thickness for strain relaxation of thin films of $PbTiO_3$ on $SrTiO_3$ at room temperature is only of the order of 10 nm when calculated using the most common approach as formulated by Matthews and Blakeslee [2](MB). Our observations as plotted in Figure 4.6 show a large discrepancy with the previous value and raises questions about the applicability of the MB model in this case. Although the MB model is widely used for ferroelectric thin films, it is not universally valid neither very appropri-

ate to describe the critical thickness of this system, since it only holds for film/substrate systems with a considerable amount of pre-existing dislocations. What is actually calculated, is the thickness at which the tension in the dislocation line is balanced by the force exerted on it by misfit stress. To ensure an existing dislocation line, a misfit of at least 0.02-0.04 [3] at the growth temperature is needed. As we just stated, the misfit strain at the growth temperature is 0.01-0.02 in our case.

The People-Bean model [3](PB), which is applicable to low misfit systems with high-quality interfaces, could be more appropriate. This model assumes that dislocations have to nucleate, which leads to a simple energy balance of the strain energy versus the energy cost of dislocation nucleation.

The misfit at the growth temperature is, thus, the key to a proper choice between the MB and the PB model. Up till now, we have used bulk literature values (as plotted in Figure 3.6 in chapter 3) to calculate these misfits. But the matter is somewhat more complicated than this simple approach. As we calculated in section 2.5.2, the T_c can be shifted up by as much as 600°C due to the strain. In Figure 4.7 temperature-dependent XRD data of a 130 nm and 280 nm $PbTiO_3$ film on $SrTiO_3$ are shown, which clearly show a shift in T_c. This effect can strongly influence the relaxation and thus the a/c-domain formation.

Using the theory as described in section 2.6.2, the critical thickness using the MB and PB model, of $PbTiO_3$ grown on $SrTiO_3$, can be calculated. Based on our TEM observations, we use Burgers vectors of type $\langle 110 \rangle$, ($\alpha = 4$, $\beta = 90°$ and $\lambda = 45°$). Other inputs are an estimate of the Poisson's ratio of 0.3, as is common to many metal oxides and the misfit strain at our typical deposition temperature of 570°C. For the $SrTiO_3$ substrate lattice parameter b, bulk values can be used [107], but a linear regression of our measurement data is probably more appropriate (and reasonably close to the literature values):

$$b_{STO} = 3.905 + 3.61 \cdot 10^{-5} T \tag{4.2}$$

with b in Å and T in °C. This is in close agreement with the bulk data provided by the supplier [72], plotted with the dash-dotted line in Figure 4.7(a).

For the $PbTiO_3$ film, we will compare the result obtained using the observed cubic (high temperature cubic parameters extrapolated down to the tetragonal phase) and tetragonal lattice parameters in these films (Figure 4.7). The cubic and tetragonal lattice parameters differ considerably and different

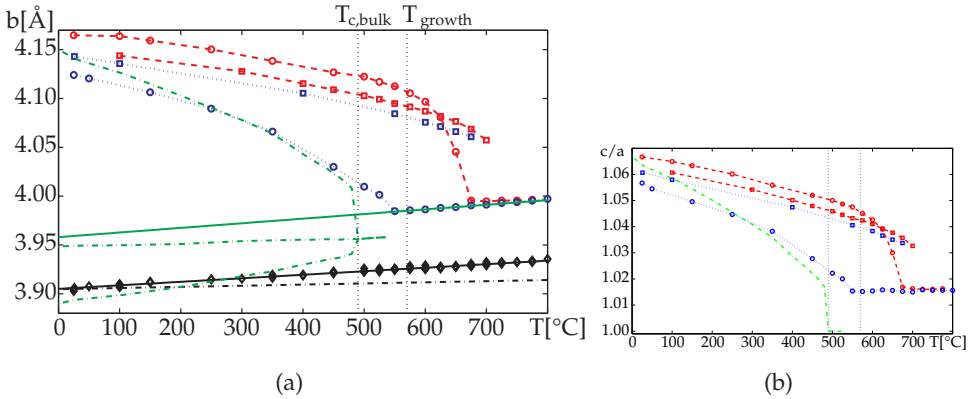

Figure 4.7: a) Temperature dependent X-ray diffraction measurements of a 130 nm thin film of $PbTiO_3$ on $SrTiO_3$: the dashed line with squares indicates the measurement during heating from room temperature; the dotted line with squares the cooling back to room temperature. Idem for a 280 nm thin film of $PbTiO_3$ on $SrTiO_3$ where the squares are replaced by circles. The solid line is a fit to the high-temperature $PbTiO_3$ measurements extrapolated into the tetragonal phase. The literature values of bulk $PbTiO_3$ by Shirane [10] (data) and Haun [13] (extrapolation) are shown by a dash-dotted line. The out-of-plane lattice parameter of cubic $SrTiO_3$ upon heating and cooling is marked by diamonds, the solid line is the fit to this measurement data. For comparison, the bulk $SrTiO_3$ data from the supplier [72] is plotted with a dash-dotted line. b) Shows the temperature dependent tetragonality of the $PbTiO_3$ thin films and bulk $PbTiO_3$, using the data from Figure a) and corresponding markers.

arguments exist to use one or the other. When one assumes that the film behaves like bulk, the cubic lattice parameters should be used. On the other hand, when one considers that the shift of T_c due to strain leads to growth of tetragonal $PbTiO_3$, the tetragonal lattice parameters should be used. For cubic $PbTiO_3$ on $SrTiO_3$ the critical thickness according to the MB and PB models is 6.2 and 48 nm, respectively. However, for tetragonal $PbTiO_3$ on $SrTiO_3$ the critical thickness according to the MB and PB models is 19 and 386 nm, respectively. The results in Figure 4.6 show that completely c-oriented $PbTiO_3$ films coherent with the substrate, can be grown up to thicknesses of at least 340 nm. This leads to two conclusions: First of all, the MB model gives too low critical thickness values and the PB gives a more realistic estimate. And

second, the film is grown directly in the tetragonal (ferroelectric) phase. Although we have not investigated it experimentally, for films with a thickness larger than the critical thickness, relaxation by misfit dislocations can still lead to only partial relaxation, leaving enough strain to shift T_c upwards and stabilize the tetragonal ferroelectric phase during growth.

Although single c-oriented $PbTiO_3$ films up to 340 nm can be grown, Figure 4.6 also shows that increased deposition rates, lead to a decrease in critical thickness. In our PLD-system, the PB model seems to hold for growth rates up to 2 Å/s (5Hz with 0.4 Å/pulse). But when the growth rate is increased, the growth imperfections and impurity phases, facilitate a/c-domain formation. This growth rate of 2 Å/s corresponds to a 5Hz laser repetition rate (with 0.4 Å/pulse) which is in good agreement with the observed relaxation time τ (Figure 4.1).

Since the a/c-domains do not order periodically, the reciprocal space maps (RSMs) as shown in Figure 4.8 reflect the relative domain orientation (tilting angles). The c- and a-domains nucleate in different places in the film and have to be able to share the strain-free (101)-plane at the domain wall. Therefore, a characteristic angle α between the c- and a-domains exists. This angle is determined solely by the c/a ratio by

$$\alpha = 90^\circ - 2tan^{-1}(\frac{c}{a}) \tag{4.3}$$

with a and c the $PbTiO_3$ lattice parameters. This angle α can be observed in RSMs by measuring the a and c lattice parameters and, redundantly, by measuring the tilt angle α, between the reciprocal lattices of the c and a domains. By measuring RSMs around different Bragg reflections, the peaks can be modeled as in Figure 4.8a-c. This gives a- and c-domains with a small difference in strain state. The a-domains are modeled using a=3.909-3.911 Å accompanied by an in-plane c=4.120-4.109 Å, where the c-value is calculated using the Poisson's ratio. The c-domains can be modeled by using c=4.140-4.121 Å and, also using the Poisson's ratio, an in-plane value of a=3.923-3.944 Å is obtained. As can be observed from the RSM, the c-domains are not tilted with respect to the substrate lattice. This gives rise to a tilt angle $\alpha = 3.01 - 2.83^\circ$ of the a-domains, in good agreement with the measurement, showing the consistency of the model.

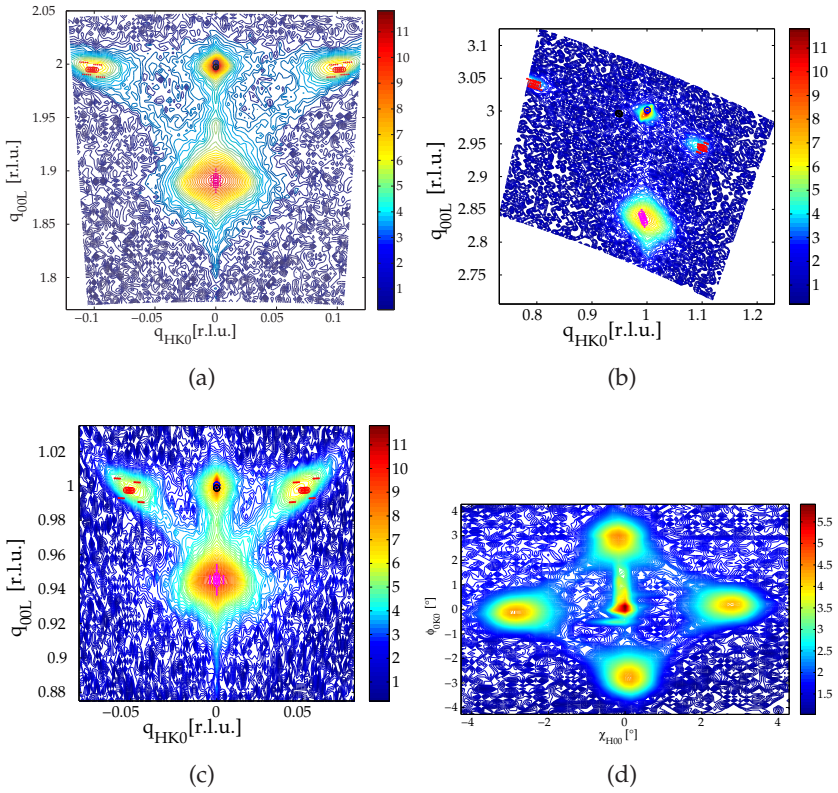

Figure 4.8: RSMs[1] in the (H0L)-plane around the (a)(002), (b)(103) and (c)(001) Bragg peak of a thick relaxed $PbTiO_3$ film on $SrTiO_3$ showing a- and c-domains. Superimposed are the peak positions of $SrTiO_3$(blue), c-domain $PbTiO_3$ (magenta) and a-domain $PbTiO_3$(black), tilted with an angle α (red). The c-domain peak is broadened corresponding to a crystal size of ∼80 nm. d) RSM in the (HK0)-plane around the (002) Bragg peak, measured in grazing incidence geometry, showing the 4-fold symmetry of the twinning domains.

4.4.2 180° domain formation

As explained previously, under the condition of a sufficiently low growth rate, single c-oriented $PbTiO_3$ thin films can be grown below the critical thickness for strain relaxation, which in the present case is very large. As

pointed out in the paragraph on Landau theory of thin ferroelectric films (specifically section 2.5.3), in determining the ferroelectric properties of these $PbTiO_3$ thin films compressively strained to $SrTiO_3$, a very important parameter is the c/a ratio. Linked to that is the T_c which, once shifted due to the strain, gives rise to a change in c/a ratio at a specific temperature. This brings us back to Figure 4.7 with the temperature-dependence of the lattice parameters and the accompanying c/a-ratio for two different thicknesses, showing different T_c values for for different thicknesses and thermal histories. The discussion of this important observation has been omitted for clarity in the previous section and will be treated here. In principle, both films are c-oriented and according to Pertsev [33] they should have similar (T_c) behavior. At room temperature, their tetragonality is indeed similar. But especially for high temperatures ($T > 500$°C) this is not the case. From their T_c-shift and lattice parameters as a function of temperature, we can thus deduce that their strain state is quite different.

Figure 4.7(a) shows that for the 280nm films the high-temperature lattice parameters do not change upon a T_c-shift from 680°C to 540°C. We can then consider that the strain state and lattice parameter of $PbTiO_3$ in the paraelectric region is well-defined. Linear regression including the well-established room temperature unstrained cubic $PbTiO_3$ lattice parameter of 3.956 Å [41], gives

$$a_0 = 3.958 + 4.73 \times 10^{-5} T \tag{4.4}$$

with a_0 in Å and T in $^\circ C$.
From the empirical equations 4.2 and 4.4, a hypothetical misfit strain u_m can be calculated and compared with the effective misfit strain obtained from the shift in T_c (section 2.5.2). The result of this comparison is shown in Table 4.1. Here, the strain state is defined as the real misfit strain, based on T_c shift, divided by the misfit strain one would expect in the ideal case when the film lattice accommodates all misfit by strain.

Table 4.1 shows that none of the c-oriented films are fully strained and that their strain states differ considerably with thickness and thermal history. Besides the differences in strain state, the most striking feature is the shift in T_c of the 280 nm film upon cooling compared to heating. The strain state of $\sim 50\%$ of the 280 nm thin film is reduced to $\sim 15\%$ after heating to 800°C, while the strain state of the 130 nm film is $\sim 90\%$, independent of heating up to 700°C. This difference is due to the larger amount of strain energy in

d [nm]	280c	280h	130
T_c [°C	550	680	850
$u_{m,TC}$	-0.002	-0.0075	-0.0142
a_0 [Å]	3.984	3.990	3.998
b [Å]	3.925	3.930	3.936
$u_{m,ab}$	-0.0151	-0.0154	-0.0159
strain state [%]	∼15	∼50	∼90

Table 4.1: Strain state calculations of $PbTiO_3$ thin films with a thickness of 280 nm (cooling (c) and heating (h)) and and 130 nm.

thicker films (strain energy scales with thickness). Therefore, the amount of thermal energy that has to be provided to overcome the energy barrier to nucleate dislocations or domain walls (and relax the strain), is obviously lower for thicker than for thinner films.

Irrespective of the strain state, 180° domains are expected in these completely c-oriented ferroelectric $PbTiO_3$ films. By careful analysis, these can be observed by XRD, as superimposed modulations in the RSM [1], [106]. Care should be taken because, as explained above, off-specular reflections and intensity modulations are also observed as a result of (relaxation) twins, multiple diffraction and diffuse scattering by dislocations. Comparing different diffraction orders is the main handle to distinguish between these different origins of off-specular peaks. Simple analysis of the first three effects shows that these can be easily distinguished. In Figure 4.9(a-c), three RSMs around the (002) Bragg peak of thin films with different thicknesses are plotted. All three show satellites along the in-plane direction, which we attribute to periodic 180° domains.

Besides, we have performed temperature-dependent synchrotron diffraction experiments, monitoring the signal around the $PbTiO_3$(001) Bragg peak, associated with the in-plane periodicity (Figure 4.9d-e). Two kinds of periodicities are observed in this case: a 20 nm periodicity which we associate with 180° domains and a 220 nm periodicity which we attribute to be induced by the terrace steps which have a similar size. By cooling down from room temperature to 10K, no measurable change in size of the two kinds of in-plane periodicity have been observed. The inertness to temperature of the terrace

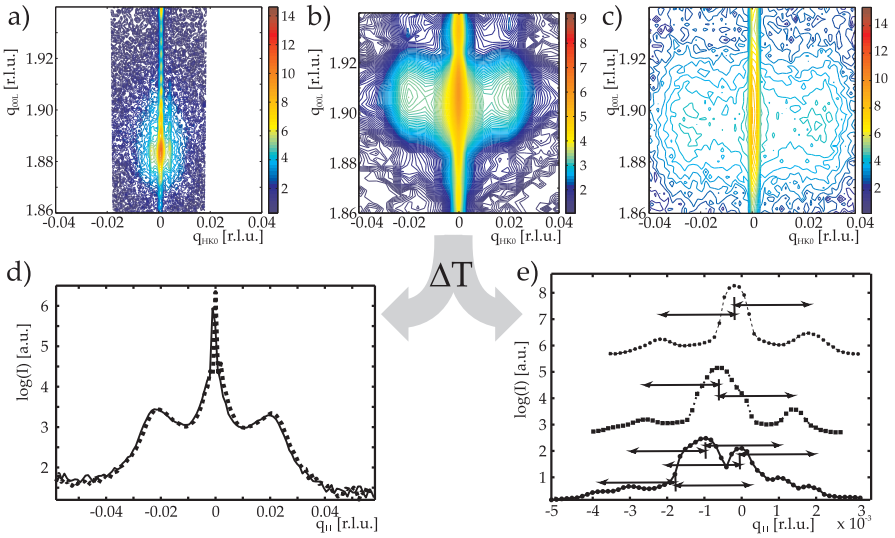

Figure 4.9: a,b,c) RSMs[1] around the $PbTiO_3$ (002) reflection of $PbTiO_3$ on $SrTiO_3$, with film thicknesses (a) 85 nm, (b) 22 nm and (c) 12 nm. The observed in-plane periodicities are respectively 107-126 nm, 19-21 nm and 13-20 nm. d) Temperature dependent XRD measurements around the $PbTiO_3$ (001) reflection of the 22 nm sample with no observable difference in the outer satellites (periodicity of 20 nm) between 300K (dotted) and 10K (solid). e) A clear change in positions of the inner satellites (220 nm). The spacing remains approximately equal but the satellites shift following the shift due to the symmetry change of the $SrTiO_3$ substrate around 105K. The top line is recorded at 150K, the middle line at 100K and the bottom line at 10K.

steps is expected with this resolution, the inertness of the polar domains with temperature probably means that at below room temperature there is no domain wall mobility and the stripes are "frozen" [50]. It is quite remarkable that Fong et al. [1] observe the disappearance of the periodic domains already above room temperature, for this thickness. This is most likely caused by the boundary conditions, as their samples are exposed to ionizing radiation for long times [108].

Note that the observed change around 105K is related to the symmetry change of the $SrTiO_3$ substrate from cubic to tetragonal. Two or three twins appear and each have their own modulations related to the in-plane periodicity of the terrace steps ($\sim$220 nm). The inertness of the 20 nm periodicity to this twinning, means that it is not strongly influenced by the substrate struc-

ture. This is an extra argument to ascribe this periodicity to the presence of periodic 180° domains, as this structural change does not change the electrical boundary conditions. In-plane measurements did not show any modulations related to a periodicity which means the domains have both periodicity and polarization perpendicular to the surface, so the periodicity can only be observed in peaks with an L-component, as expected (see equation 3.5).

Although in the direction normal to the film/substrate interface, the "up"

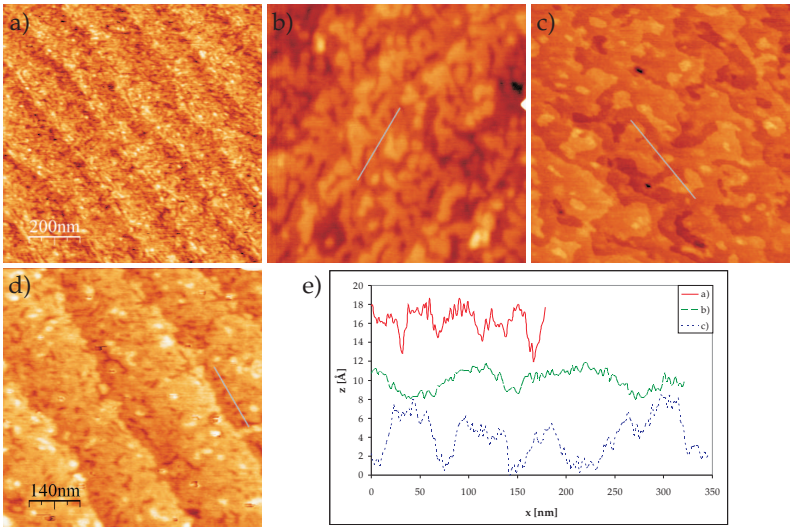

Figure 4.10: AFM images of $PbTiO_3$ thin film with (b+c) and without (a+d) buffer electrode $SrRuO_3$ layer on $SrTiO_3$. The layer thicknesses in a+d) are 22 nm ($PbTiO_3$), b) 4 nm ($PbTiO_3$), 45 nm ($SrRuO_3$) and c) 5 nm ($PbTiO_3$), 5 nm ($SrRuO_3$). The full z-scale of all images is 2 nm, the scan size of a-c is 1x1μm. e) shows the line profile of the sections as indicated in the scans.

and "down" domains in a 180° domain structure have equal thicknesses, these domains can possibly be observed by AFM. We have observed minute contrast in AFM scans on thin films with a very flat unit-cell step morphology (Figure 4.10a+d). It is remarkable that the height contrast is 2-3 Å, close to approximately half a unit cell. Growth effects usually show height contrast close to 4-5 Å, a full unit cell. Comparing different surfaces of $PbTiO_3$ does not show very distinctive differences in height contrast. Figure 4.10 a) and d) most likely show 180° domains, whereas b) and c) show unit cell steps

imaged with a blunt (b) and sharp (c) tip. From our observation, it can not be ruled out that the contrast is due to another effect than 180° domains. But there is a strong resemblance to the recent observations by Thompson et al. [108], who ascribe this to the presence of $180°$ domains. They state that the contrast mechanism is not yet clear, but at least two possible mechanisms exist: One is related to the electrostatic interactions between the tip and the near-surface electric fields of the domains or their adsorbates. The other is based on the small intrinsic height differences between the positively and negatively charged adsorbates attached preferentially to each polarization orientation.

Altogether, this leads to the conclusion that the observations as in Figure 4.9 and 4.10 are signatures of the thin films being ferroelectric, consisting of ordered $180°$ domains. Still, direct measurements of a ferroelectric response would be desirable and has been attempted in next section.

4.4.3 Electrical properties

Our AFM and XRD observations indicate that thin films of $PbTiO_3$ on $SrTiO_3$ can be ferroelectric, strained and single oriented. In such a system, ferroelectric $180°$ domains are expected and in the previous paragraph, we have shown observations of these domains. These signatures of being ferroelectric are not directly confirmed by electrical measurements. Actually measuring the ferroelectric response of thin films of pure $PbTiO_3$ is problematic due to the fact that it behaves often as a semiconductor [97] and that interface effects play a large role in the measurement [121]. Using bottom $SrRuO_3$ and top Au electrodes, we have not succeeded to measure ferroelectric hysteresis loops on thin films of approximately 30 nm $PbTiO_3$ with macroscopic electrodes. These measurements are extremely sensitive to workfunction matching and interface layers. To our knowledge, only very few reports on ferroelectric loops using macroscopic electrodes on $PbTiO_3$ thin films with thicknesses down to 2 nm exist [105]. These measurements have been performed using $Nb : SrTiO_3$ substrates or $SrRuO_3$ bottom electrodes and Pt top electrodes.

In order to show the potential of ferroelectric thin films compared with bulk ferroelectrics, we have measured ferroelectric hysteresis loops using macroscopic electrodes on relatively thick PZT samples in cooperation with

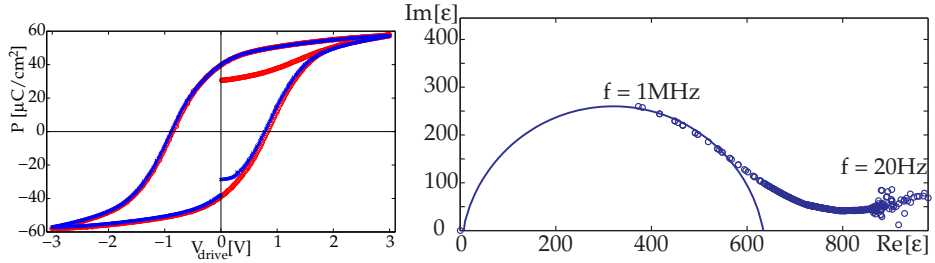

(a) (b)

Figure 4.11: a) Standard bipolar hysteresis loops measured with a 20ms hysteresis period and 1000ms preset delay on a 100 nm PZT thin film on $SrTiO_3$ with top and bottom $SrRuO_3$ electrodes. The circles correspond to a measurement on a "fresh" electrode (first measurement), while the crosses mark a second measurement on this electrode (pre-poled). This shows the sample is pre-poled with a positive bias. b) Cole-Cole plot of the real and imaginary part of the dielectric constant of a thin film of 100 nm PZT. Indicated are the limiting measurement frequencies. The fitted semi-circle corresponds to a static dielectric constant $\epsilon' = 640$.

Joost van Bennekom [3]. The piezoelectric voltage-polarization hysteresis loop shown in Figure 1.3 is measured on a ceramic PZT sample with a thickness of 790 μm. Voltage sweeps with increasing maximum field have indicated the requirement of a minimum field for proper switching. The main parameters which can be obtained from these loops are the coercive field, $E_c = 7.3kV/cm$, and a remanent polarization, $P_r = 26\mu C/cm^2$. The good switching and remanence are measured using voltages up to $1.9kV$, which shows the drawback of these bulk-like samples: the high switching voltages. A decrease of thickness to 100 nm, without changes in materials' properties could reduce this to a voltage of $0.25V$.

In cooperation with Arjen Janssens[4] we have performed macroscopic ferroelectric measurements on thin films of PZT with $SrRuO_3$ bottom and top electrodes. A typical hysteresis loop on a 100 nm PZT film is shown in Figure 4.11. The remanent polarization $P_r = 38.8 \pm 1.1\mu C/cm^2$ is 50% larger than

[3]University of Twente, currently at University of Groningen, The Netherlands

[4]PhD in the Inorganic Materials Science group at the University of Twente, the Netherlands.

that of bulk PZT treated in the previous paragraph. The coercive voltage, $V_c \approx 0.83 \pm 0.05V$, which corresponds to a coercive field, E_c (d=100 nm), of $83 \pm 5kV/cm$, is more than a factor 10 larger than that of bulk PZT. Still, the applied voltage is relatively low. The increase in coercive field with decreasing thickness is well known [45]. The difference in remanent polarization is most likely to be ascribed to the difference in microstructure. Although PZT grows in a columnar fashion as a thin film, it is highly oriented, whereas the bulk material is randomly oriented. Frequency dependent dielectric measurements on this 100 nm PZT sample indicate a static dielectric constant ϵ' of 640 ± 100 (see Figure 4.11). Besides, this measurement shows that this large value is associated to a relaxation mechanism with a characteristic frequency of about 1 MHz (see fitting semicircle), most likely the relaxation of domain walls.

On thin films of $PbTiO_3$ on $SrTiO_3$, only microscopic functional mea-

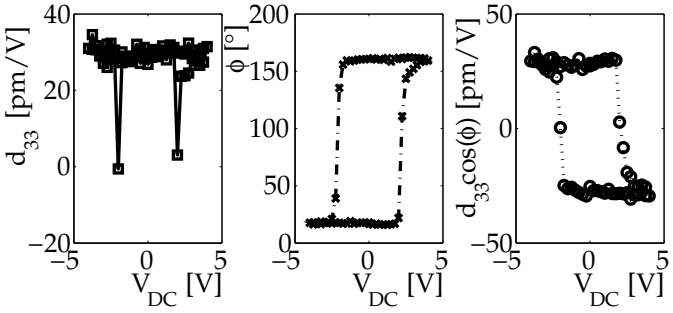

Figure 4.12: Piezoelectric characterization of sample A (see Table 4.2) by p-AFM. From left to right: measured d_{33}, measured phase and the effective d_{33} calculated from those measurements.

surements have been performed, by Alessio Morelli [99]. Piezoresponse-AFM (p-AFM) allows for ferroelectric measurements without macroscopic (top)electrodes, considerably reducing possible leakage paths and changing the interface effects (which are still present). Acquiring quantitative parameters from these measurements is complex due to the unknown contact effects and inhomogeneous electric field due to the tip shape, but an effort has been done in this direction, as presented in figure 4.12. Most measurements show switching behavior and statistics over a large number of measurements

	A	B	C
E_c [kV/cm]	150	420	400
d_{33} [pm/V]	30-33	10-30	10-35

Table 4.2: Overview of the coercive field E_c and piezoelectric coefficient d_{33} of sample A: 130 nm $PbTiO_3$ on 30 nm $SrRuO_3$ on $SrTiO_3$; B: 100 nm $PbTiO_3$ on 40nm $SrRuO_3$ on $SrTiO_3$ and C: 110 nm $PbTiO_3$ on 40 nm $SrRuO_3$ on $SrTiO_3$.

(5-50) on every sample, shows that the coercive field is E_c=150-420 kV/cm. The factor of 2-4 difference with the coercive fields observed in macroscopic measurements, is most likely caused by imperfect contact and the inhomogeneous field due to the tip shape.

Using a force curve calibration, the microscope has been calibrated to perform d_{33} measurements. The d_{33} and the effective $d_{33} \cdot cos(\theta)$ measured in this way (without any further corrections), are plotted in Figure 4.12. In this case $d_{33} \approx 30$ pm/V, but in general, the d_{33} value shows a large spread from 10 to 35 pm/V (Table 4.2). Compared to the $d_{33} = 79.1pm/V$ as calculated for single crystals [13], this value is somewhat low. But at room temperature, a decrease in d_{33} is expected for $PbTiO_3$ thin films strained on $SrTiO_3$ (compressive $u_{m,cub}$) [122]. Based on the large T_c shifts that we observe, the effective stress is such that it can lead to a considerable decrease in d_{33}.

Quantitative verification of the d_{ij} coefficients is known to be difficult, since the measured signals are generally small and thorough measurement calibration is required. Therefore, reports of experimentally determined d_{33} values are very scarce in literature and our observation is of the same order of magnitude as the few values reported: Tandon et al. show a value converging to $d_{33} \approx 50pm/V$ [123]. Besides, retention times of these films are in the order of 100 hours, which is in close agreement with other reports [55].

4.5 Conclusions

First of all, our study confirms the accepted knowledge that the thermal history of a ferroelectric determines its domain configuration. At the typical growth temperature we have employed for thin films of $PbTiO_3$ on $SrTiO_3$ (570°C), the growth takes place directly in the tetragonal phase. This is due to

the misfit strain between substrate and film, which gives rise to a shift in T_c, in accordance with Pertsev's theory [33]. Unlike many previous reports, we have shown that the self-strain of the $PbTiO_3$ has to be taken into account to calculate the critical thickness of these thin films on $SrTiO_3$. In other words, we provide a physical explanation for the T_c shift as predicted by a Landau approach [33]: it is energetically not favorable for the $PbTiO_3$ to be in the cubic phase with large internal stresses. Instead, it is energetically favorable for the film to grow in the tetragonal phase (which although it is not the ground state of the bulk material at the growth temperature, it is relatively close in energy), in order to achieve coherency.

Moreover, we have shown that the Matthews-Blakeslee model (MB) does not predict the critical thickness for strain relaxation in these thin films properly. In many cases, the MB model is appropriate, but in this case it is much more realistic to use the model by People and Bean (PB). This last model does not only predict a critical thickness in much better agreement with our observations, but the assumptions at the foundations of the model are also much better met: The MB model uses assumptions which imply that interfacial misfit dislocations only form in the presence of grown-in threading dislocations [3]. But for very small misfits, very few threading dislocations are expected and thus this mechanism is expected not to be a source of misfit dislocations. The PB model is based on an energy balance which assumes the initial absence of misfit dislocations and their formation when it is energetically favorable. When grown in the tetragonal state, MB predict a critical thickness of 19 nm, while PB predict 386 nm. This explains the successful growth of single domain dislocation-free thin film with thickness above 100 nm reported in some instances in the literature [124], for which the mechanism of the large critical thickness remained unexplained up to now, as well as our own results.

Indeed, we have slowly grown films with thicknesses up to 340 nm and did not observe any relaxation by a-domain formation, which supports the PB model. Note that this observation has large consequences for the interaction between modeling and experimental observations of ferroelectric thin films. The difference in conception of the lattice misfit has already been mentioned in chapter 1 and in models [42], the critical thickness is usually calculated using the cubic state of $PbTiO_3$ and the MB model.

Another important parameter determining the domain structure is extrin-

sic to the $PbTiO_3/SrTiO_3$ system: the growth rate. When films are grown rapidly, in the case of our PLD system typically at laser repetition rates above 5Hz and 0.4 Å/pulse growth rate (i.e. 2 Å/s), a-domains form. This domain formation is accompanied and probably triggered by growth imperfections and off-stoichiometry. These a-domains form a crystallographic twin structure with c-domains (sharing the strain-free (101)-plane). For thick and rapidly grown films, we have been able to determine the characteristic twin angle $\alpha = 2.92 \pm 0.09°$. This is somewhat smaller than the value observed in bulk ($\alpha = 3.57°$), which indicates the presence of tensile stress on c-domains and/or compressive stress on a-domains. This means that compared to the self-strained bulk $PbTiO_3$, the c-domains are tensile strained in-plane. But with respect to the cubic $PbTiO_3$, the c-domains are still compressively strained in-plane.

For single c-oriented films, periodic 180° domains are observed both by AFM and XRD. The contrast mechanism of these 180° domains in AFM is still not clear and it is hard to distinguish the probable observation of 180° domains from unit cell steps due to two-dimensional growth.

The good coherence and high substrate/film interface quality is confirmed by double diffraction or "Umweganregung". Although double diffraction is often not taken into account or misinterpreted in XRD measurements, we show that these diffraction peaks can be used as a powerful method to study closely matched epitaxial systems.

Besides all the qualitative measurements of the ferroelectric properties of thin films of $PbTiO_3$, also quantitative functional measurements have been performed. The large leakage and strong interface effects, prevented us from performing macroscopic electrical measurements. p-AFM does allow for local functional measurements. Alas, this method shows a large variation in the measurement values, mainly due to varying sample regions and tip/surface contacts. Still, a piezoelectric coefficient d_{33} of ~ 30 pm/V has been measured and single c-oriented thin films of $PbTiO_3$ have been shown to display long retention times in the order of 100hrs.